Linking structure to fragility in bulk metallic glass-forming liquids

Linking structure to fragility in bulk metallic glass-forming liquids

Shuai Wei,[1,2,a),b)] Moritz Stolpe,[1,a)] Oliver Gross,[1] Zach Evenson,[1,3] Isabella Gallino,[1] William Hembree,[1] Jozef Bednarcik,[4] Jamie J. Kruzic,[5] and Ralf Busch[1]

[1]*Department of Materials Science and Engineering, Saarland University, Campus C63, 66123 Saarbrücken, Germany*
[2]*Department of Chemistry and Biochemistry, Arizona State University, Tempe, Arizona 85287, USA*
[3]*Institut für Materialphysik im Weltraum, Deutsches Zentrum für Luft- und Raumfahrt (DLR), 51170 Köln, Germany*
[4]*Deutsches Elektronen-Synchrotron DESY, Notkestrasse 85, D-22603 Hamburg, Germany*
[5]*Material Science, School of Mechanical, Industrial, and Manufacturing Engineering, Oregon State University, Corvallis, Oregon 97331, USA*

Using *in-situ* synchrotron X-ray scattering, we show that the structural evolution of various bulk metallic glass-forming liquids can be quantitatively connected to their viscosity behavior in the supercooled liquid near T_g. The structural signature of fragility is identified as the temperature dependence of local dilatation on distinct key atomic length scales. A more fragile behavior results from a more pronounced thermally induced dilatation of the structure on a length scale of about 3 to 4 atomic diameters, coupled with shallower temperature dependence of structural changes in the nearest neighbor environment. These findings shed light on the structural origin of viscous slowdown during undercooling of bulk metallic glass-forming liquids and demonstrate the promise of predicting the properties of bulk metallic glasses from the atomic scale structure. © 2015 AIP Publishing LLC.
[http://dx.doi.org/10.1063/1.4919590]

The supercooling of liquids and formation of glasses are crucial for various fields, such as optical science, food processing, life science, and engineered amorphous solids.[1–4] The ability of a liquid to readily form a glass depends on both thermodynamic and kinetic factors. While thermodynamics determine the driving force for crystallization, kinetics reflect the rate at which the underlying atomic processes proceed. The latter can be studied on the macroscopic level through measurements of the liquid's viscosity η. Among glass-forming liquids, the temperature dependence of viscosity can vary considerably.[1,4–6] While some liquids follow an Arrhenius law (strong liquids), others display non-Arrhenius behavior (fragile liquids). A quantitative description of the diversity of kinetic behavior is the notion of fragility as proposed by Angell.[1,5] Fragility quantifies the temperature dependence of viscosity and can be described by the empirical Vogel-Fulcher-Tammann (VFT) equation,[1,2] $\eta = \eta_0 \exp[D^*T_0/(T - T_0)]$, where η_0 is the theoretical infinite-temperature limit of viscosity and T_0 is the temperature at which barriers to viscous flow in the supercooled liquid would approach infinity. D^* describes the deviation from Arrhenius behavior and smaller D^* values correspond to more fragile liquids. Fragility can be alternatively represented by the steepness index,[1,5] m, defined as the logarithms slope of viscosity at T_g via $m = d\log \eta / d(T_g/T)|_{T=T_g}$. The relation between m and D^* is given by $m = m_{\min} + m_{\min}^2 \cdot \ln 10/D^*$, where $m_{min} = \log(\eta_g/\eta_0)$ and $\eta_g = 10^{12}$ Pa s (Refs. 1 and 5). Larger m values (smaller D^*) indicate more fragile behavior.

Adam-Gibbs theory[7] connects the kinetic behavior of liquids to their thermodynamic properties (e.g., configurational or excess entropy[8,9]). The potential energy landscape links both properties to the inherent structure of liquids.[2,10,11] Furthermore, fragility influences the mechanical properties of the glassy state such as the fracture energy, ductility, and Poisson's ratio, υ,[12] the latter of which has been shown to correlate to the atomic packing density.[13] Thus, the current understanding suggests a mechanistic connection between the fragility and atomic scale structure. Although some insights have been gained,[14–16] a quantitative description of this connection has not been elucidated.

The main challenge in relating fragility to a liquid's structure lies in precisely defining the characteristic structural parameters of fragility. Such a parameter should describe the temperature dependent evolution of structure, as fragility reflects the temperature dependence of viscosity. *In-situ* synchrotron X-ray scattering allows for precise and rapid measurements of the glass and supercooled liquid structure with high spatial and temporal resolutions. This technique is therefore ideal for resolving the real-time structural changes in bulk metallic glasses (BMGs) as a function of temperature and allows us to quantitatively link atomic scale structure and fragility. We investigated seven multicomponent systems based on Zr, Au, and Pt, which comprise a wide range of fragility among BMG-forming liquids (see Table I for compositions and detailed methods in supplementary material[17]). Fragilities were determined in the previous work[18–24] at temperatures near T_g using three-point beam bending viscosity measurements (see Table I).

The structural metrics correlating with fragility in this work are established in the supercooled liquid state (above the glass transition zone). In the supercooled liquid state, the

---
a)Authors to whom correspondence should be addressed. Electronic addresses: shuai.wei@asu.edu and m.stolpe@mx.uni-saarland.de.
b)Present address: Department of Chemistry and Biochemistry, Arizona State University, Tempe, Arizona 85287, USA.

TABLE I. Summary of structural and kinetic fragilities for the measured systems. The D^* values were determined from viscosity data fits of the VFT equation with $\eta_0 = 4 \times 10^{-5}$ Pa s.

Composition (at. %)	D^*	m	$1/m_{str}^{(r1)}$	$m_{str}^{(r4)}$	$m_{str}^{(V4-3)}$	T_g' (K)
$Pt_{60}Cu_{16}Co_2P_{22}$ (Pt60)	10.8[a]	73.7	292.4	0.0387	0.0936	520
$Pt_{42.5}Cu_{27}Ni_{9.5}P_{21}$ (Pt42)	15.3[b]	56.9	173.9	0.0204	0.0455	531
$Au_{49}Cu_{26.9}Si_{16.3}Ag_{5.5}Pd_{2.3}$ (Au49)	16.9[c]	53.0	122.9	0.0184	0.0319	408
$Zr_{52.5}Cu_{17.9}Ni_{14.6}Al_{10}Ti_5$ (Vit.105)	18.6[d]	49.7	103.4	0.0136	0.0207	703
$Zr_{59.3}Cu_{28.8}Al_{10.4}Nb_{1.5}$ (AMZ4)	24.8[e]	41.4	79.5	0.0121	−0.0001	694
$Zr_{58.5}Cu_{15.6}Ni_{12.8}Al_{10.3}Nb_{2.8}$ (Vit.106a)	21.0[f]	45.9	66.0	0.0102	0.0064	708
$Zr_{44}Ti_{11}Ni_{10}Cu_{10}Be_{25}$ (Vit.1b)	25.4[g]	40.8	103.0	0.0138	−0.0018	661

[a]Reference 18.
[b]Reference 23.
[c]Reference 21.
[d]Reference 20.
[e]Reference 24.
[f]Reference 22.
[g]Reference 19.

system re-attains its metastable equilibrium state (fully relaxed) and structural relaxation times fall below the experimental time scale. Therefore, the analysis of the metastable equilibrium regime avoids the effect of non-equilibrium relaxation that plays a role at or below the glass transition. In other words, physical properties and structure do not depend on thermal history or initial states anymore. There is a practical advantage of using as-cast samples that the system upon heating reaches its supercooled liquid regime without a "overshoot" (deviation shortly from the equilibrium before stabilizing), which enables a wider range of the data collected in the metastable equilibrium state, resulting a better quality of fitting.

The experimentally determined total X-ray structure factors $S(Q)$ are converted into real space information using Fourier transformation (see supplementary material Methods[17]). As a result, one directly obtains the total reduced pair distribution function (PDF) $G(r)$, which is related to the total PDF $g(r)$ and the total pair density function $\rho(r)$ via $G(r) = 4\pi r\rho_0 [g(r) - 1] = 4\pi r [\rho(r) - \rho_0]$, where r is the distance and ρ_0 is the average number density.[17,25] The total $G(r)$ consists of multiple partial reduced PDFs and is difficult to accurately decompose for four or five component systems. However, the dominant contributions to $G(r)$ are those atomic spatial correlations of the majority atomic species with large scattering lengths (e.g., Zr, Pt, and Au).[25] The shifts of the i-th peak position, r_i, of $G(r)$ can be interpreted in terms of the corresponding shifts of $g(r)$, as the correlation analyses of $G(r)$ in the following lead to qualitatively equivalent results as $g(r)$ (see supplementary text and Fig. S1 in supplementary material[17]).

To quantify the structural changes with temperature, we determine the shift of r_i of $G(r)$ (see Fig. 1(a)). Figure 1(b) shows the evolution of r_1 with respect to its value at 323 K; r_1 exhibits a sudden slope change at the glass transition coinciding with the jump in heat flow measured using differential scanning calorimetry (DSC) (see inset). Arrows indicate the onset temperature of the supercooled liquid region, T_g', as observed in DSC upscans (Table I). As the supercooled liquid region is reached, r_1 decreases with increasing temperature. In order to establish a metric relating the liquid's

structural changes to its kinetics, we examine the change in $r_1(T)$ with respect to its value at T_g', $\Delta r_1(T)/r_1(T_g')$ $= [r_1(T) - r_1(T_g')]/r_1(T_g')$. By plotting these data on a T_g'/T scale (Fig. 1(c))—similar to Angell's fragility plot—we notice that as T_g' is approached, fragile liquids (small D^*) consistently exhibit a slower rate of change in r_1 than strong liquids (large D^*).

For a quantitative comparison similar to the steepness index of fragility, we define the *structural fragility*, $m_{str}^{(r1)}$, as the slope of the structural data from r_1 at T_g' in Fig. 1(c)

$$m_{str}^{(r1)} = \{d[\Delta r_1(T)/r_1(T_g')]/d(T_g'/T)\}|_{T=T_g'}. \quad (1)$$

Accordingly, $m_{str}^{(r1)}$ is determined by a linear fit of the data in the range from $T_g'/T = 0.9$ to 1 and listed in Table I. Figure 1(d) shows that $1/m_{str}^{(r1)}$ correlates to kinetic fragility, m, via $m_{str}^{(r1)} = 1/(6.48m - 200)$ with an adjusted $R^2 = 0.880$.

Above T_g', r_1 decreases for all studied alloys. This behavior is a common observation in metallic liquids.[26] Lou *et al.* assigns this negative shift to a decrease in coordination number, which they attribute to the formation of more densely packed atomic clusters at higher temperatures.[27] However, we find no significant change in the apparent coordination number from T_g' up to the onset temperature of crystallization (Fig. S2 in supplementary material[17]). An alternative explanation has been proposed by Ding *et al.*[26] According to their computations at constant coordination number, a negative shift in r_1 can arise simply from the thermally induced redistribution of the relative atomic position with respect to the inherent liquid structure and results from the asymmetry of the interatomic potential.[26] Our results show that this shift is more pronounced for strong than for fragile liquids (see Fig. 1(c)).

Corresponding analysis of the 2nd, 3rd, 4th, and 5th peak positions of $G(r)$ (Fig. S3 in supplementary material[17]) reveals that only r_4 correlates with fragility as shown in Fig. 2. In contrast to the behavior of r_1, r_4 increases with increasing temperature (see Fig. 2(a)). The results of the T_g'-normalized shift of the 4th peak, $-\Delta r_4(T)/r_4(T_g')$ plotted against T_g'/T are displayed in Fig. 2(b). Approaching T_g', fragile liquids demonstrate a more rapid change in r_4 than
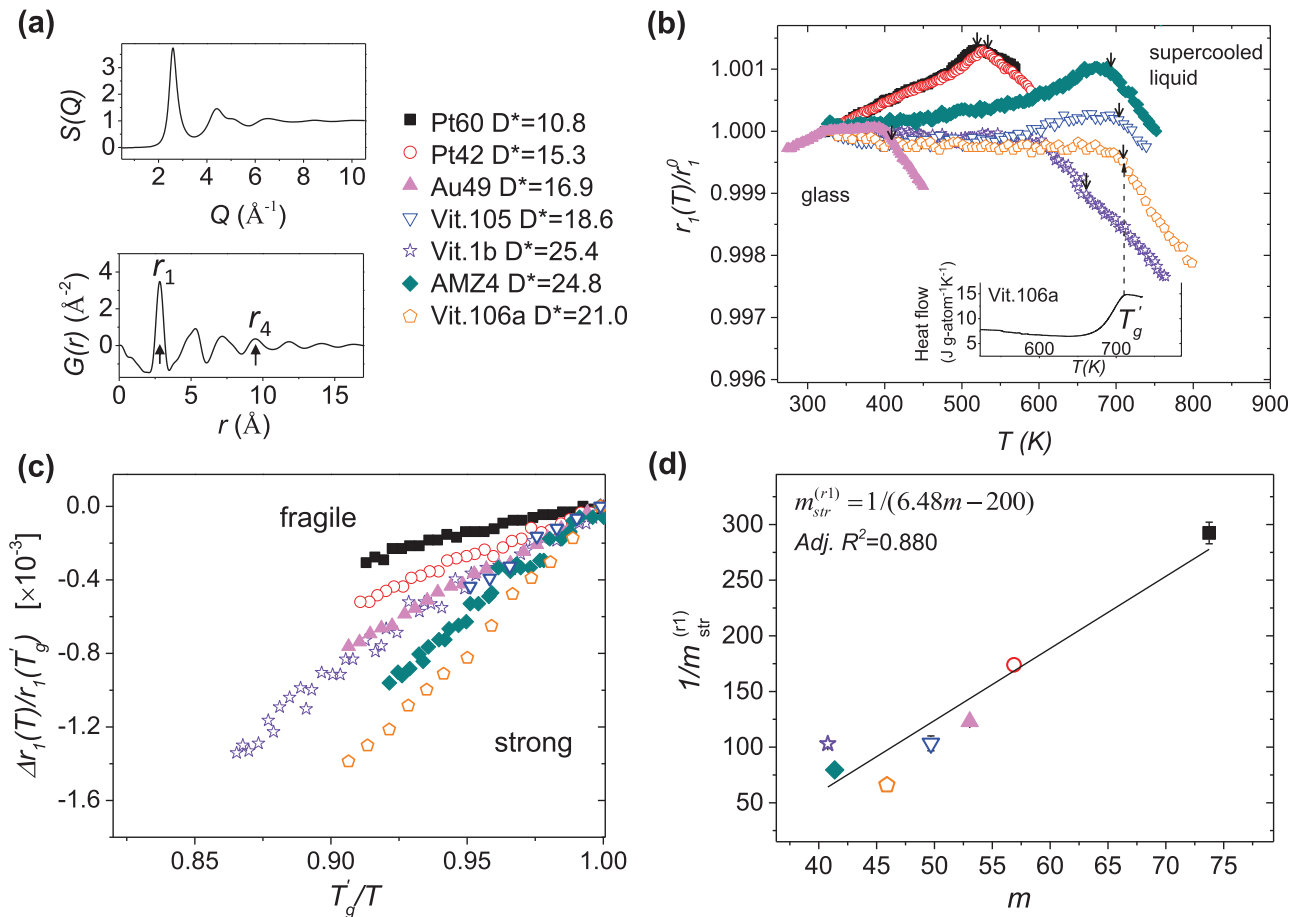
FIG. 1. *In-situ* synchrotron x-ray scattering measurement upon heating. (a) An example of total structure factor, $S(Q)$, and reduced pair distribution function, $G(r)$, in this case for AMZ4. r_1 and r_4 indicate the 1st and 4th peak positions of $G(r)$, respectively. (b) The changes in the first peak position, r_1, of $G(r)$ normalized to the value r_1^0 at 323 K. The sudden slope change is due to the glass-to-liquid transition. r_1 decreases with increasing T in the supercooled liquid state. Arrows indicate T_g' for the respective alloys. Inset: DSC heat flow of as-cast sample of Vit.106a throughout the glass transition on the same temperature scale. The dashed line shows that the end of calorimetric glass transition coincides with the T_g' of Vit.106a (arrow on orange pentagon). (c) The changes in r_1 are scaled to $\Delta r_1(T)/r_1(T_g')$ and plotted on a T_g'/T scale. A fragile liquid tends to have a small change of r_1 with respect to $r_1(T_g')$. (d) The inverse structural fragility $1/m_{str}^{(r1)}$ vs. the kinetic fragility m. Error bars represent the standard deviation from fitting and the solid line is a linear fit. Alloys are designated by symbol color.
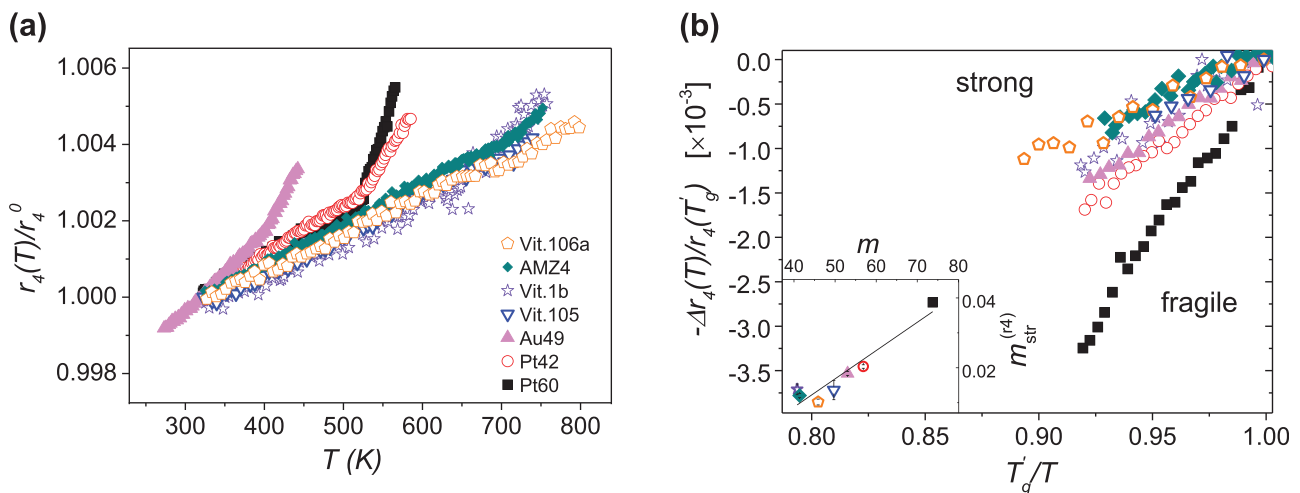

FIG. 2. Structural changes on medium-range order length scales. (a) The changes in the 4th peak position, r_4, of $G(r)$ normalized to the value r_4^0 at 323 K. (b) The changes in r_4 normalized to T_g'. Colored symbols represent different alloys as indicated in the legend of (a). The changes in r_4 approaching T_g' tend to be steeper for kinetically fragile liquids compared with strong liquids. Note that the negative sign for r_4 is used to analogize the Angell-plot of viscosity. Inset: The structural fragility $m_{str}^{(r4)}$ vs. kinetic fragility m. Error bars represent the standard deviation from fitting.

strong liquids, showing an inversed pattern as r_1 does (Fig. 1(c)). Similar to our treatment of r_1, we define a structural fragility parameter for r_4 as

$$m_{str}^{(r4)} = \{d[-\Delta r_4(T)/r_4(T_g')]/d(T_g'/T)\}|_{T=T_g'}. \quad (2)$$

The results of linear fitting from $T_g'/T = 0.9$ to 1 are listed in Table I. The inset of Fig. 2(b) shows a positive correlation between $m_{str}^{(r4)}$ and m with $R^2 = 0.880$ (assuming a linear relation $m_{str}^{(r4)} = 8.10 \times 10^{-4} m - 0.024$).

Assuming that r_i represents the average distance of the i-th coordination shell, the corresponding volume sphere up to r_4 is $V_4(T) = \frac{4}{3}\pi r_4^3(T)$. The change in $V_4(T)$ normalized to T_g' can then be regarded as the thermally induced "volume dilatation," $\varepsilon_4 = -\Delta V_4(T)/V_4(T_g')$ on a length scale $r \leq r_4$. Accordingly, the shift of r_4 due to broadening of $G(r)$ reflects the thermally induced volume increase at all $r \leq r_4$. Within this volume, no remarkable change in average number of enclosed atoms was observed with varying temperature (Fig. S2 in supplementary material[17]). Indeed, this volume description with V_4 leads to an almost identical correlation with fragility, as that revealed by r_4 (see Fig. S4 in supplementary material[17]).

To understand the origin of the correlation between V_4 (or r_4) and fragility, we section V_4 into spherical *volume shells*, $V_{i-j} = V_i - V_j = \frac{4}{3}\pi(r_i^3 - r_j^3)$, where $j = 0$, 1, 2, 3, $i = j + 1$ (defining $r_0 \equiv 0$) ,and calculate the corresponding volume dilatation, $\varepsilon_{i-j} = -\Delta V_{i-j}(T)/V_{i-j}(T_g') = -[V_{i-j}(T) - V_{i-j}(T_g')]/V_{i-j}(T_g')$. In doing so, we gain knowledge about the spatial distribution of the thermally induced volume changes in each volume shell, which allows us to more precisely identify the length scale of the structural changes that determines fragility. The obtained ε_{i-j} varies among different volume shells, suggesting a heterogeneous distribution of the thermally induced volume. Remarkably, among ε_{2-1}, ε_{3-2}, and ε_{4-3}, only the dilatation ε_{4-3} correlates with fragility, as shown in Fig. 3(a), whereas others do not (Fig. S5 in supplementary material[17]). Defining $m_{str}^{(Vi-j)}$ as

$$m_{str}^{(Vi-j)} = d\varepsilon_{i-j}/d(T_g'/T)|_{T=T_g'}, \quad (3)$$

we obtain a consistent linear correlation between the rate of V_{4-3} dilatation, $m_{str}^{(V4-3)}$, and fragility m, via $m_{str}^{(V4-3)} = 2.95 \times 10^{-3} m - 0.124$ with an adjusted $R^2 = 0.993$, as shown in Fig. 3(b).

This excellent correlation suggests that the fragility of viscous metallic liquids is determined by the structural evolution on a length scale of about 3 to 4 atomic diameters (~ 1 nm). We interpret this as the thermally induced dilatation of the structure resulting from the "incorporation" of volume between the 3rd and 4th coordination shell. The larger the increase in the volume on this scale with respect to its value at T_g' upon heating, the faster the viscosity decreases, thus, the higher the fragility (see Fig. 3). According to experimentally supported[28] structural models of metallic glasses,[29,30] atomic clusters and their spatial arrangements form short- and medium-range order. While distorted clusters are considered as sources of higher mobility, the formation of less mobile ("solid-like" or slow) regions through energetically favored *regular* polytetrahedral clusters (with minimum disclinations) is considered to slow down the dynamics.[14] Our finding shows that the length scale associated with fragility extends beyond a single cluster size (~ 3 atomic diameter), thus corresponding to inter-cluster correlations and representing medium-range order.[14] In this regard, the dilatation between the 3rd and 4th coordination shell can be interpreted as the key structural signature of medium-range ordering through efficient packing of those *regular* clusters. This supports the idea that structural heterogeneities, inducing dynamic heterogeneities,[2,14,31] are responsible for the viscous slowdown of supercooled liquids.

In summary, we establish a quantitative connection between structural changes and kinetics in metallic glass-forming liquids. For strong liquids, the temperature dependent structural changes are more pronounced in nearest neighbor atomic environment. Meanwhile, for fragile liquids, remarkable structural changes are observed on the length scale of the
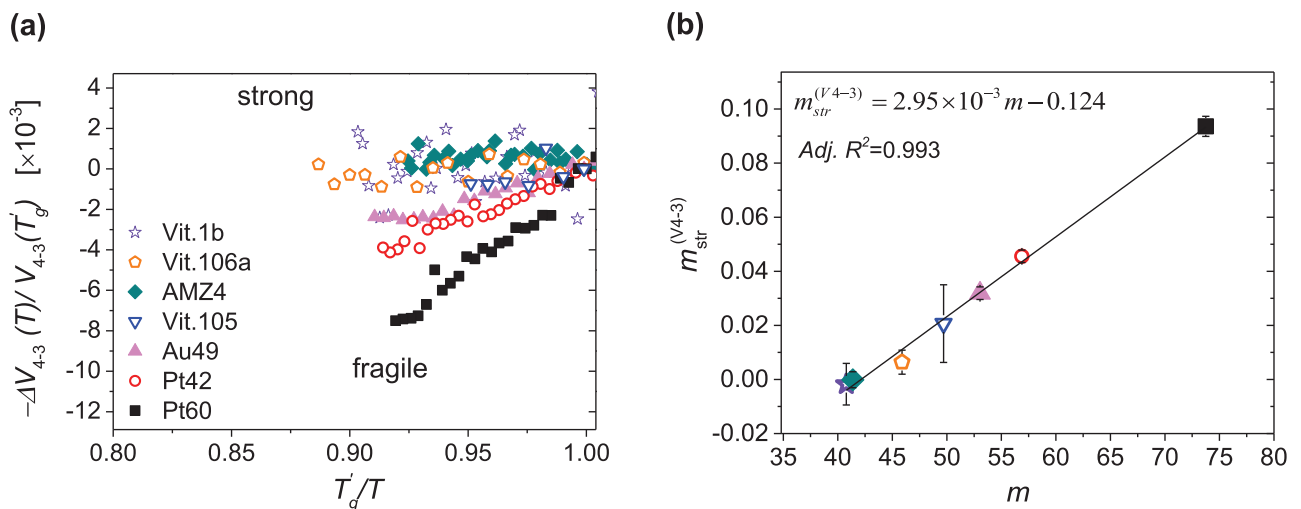
(a)

(b)

FIG. 3. Structural evolutions of strong and fragile liquids represented by volume dilatation, ε_{4-3}, corresponding to the local volume V_{4-3} changes between r_3 and r_4. (a) The diverse behavior of thermally induced volume within the spherical volume shell between r_3 and r_4. Fragile liquids show a faster incorporation of the induced volume with respect to temperature upon heating. Strong liquids exhibit a slower increase in the volume. (b) The structural fragility $m_{str}^{(V4-3)}$ correlates excellently with kinetic fragility m. Error bars are standard deviation of fitting. Colored symbols represent different alloys (see the legend of (a)). The solid line is a linear fit.

3rd to 4th coordination shell ($\sim$1 nm) and, specifically, larger thermally induced volume dilatations on this length scale lead to more fragile behavior. Based on the established relationships between fragility, thermodynamics,[8–10] and mechanical properties,[12] the derived structural parameters are consequently linked to the entropy of liquids and the Poisson's ratio of glasses, which are useful for predicting and tailoring physical properties of amorphous materials by engineering of the atomic-scale structure.

[1] C. A. Angell, Science **267**, 1924 (1995).
[2] P. G. Debenedetti and F. H. Stillinger, Nature **410**, 259 (2001).
[3] J. Schroers, Phys. Today **66**(2), 32 (2013).
[4] J. Orava, L. Greer, B. Gholipour, D. W. Hewak, and C. E. Smith, Nat. Mater. **11**, 279 (2012).
[5] R. Bohmer, K. L. Ngai, C. A. Angell, and D. J. Plazek, J. Chem. Phys. **99**, 4201 (1993).
[6] R. Busch, J. Schroers, and W. H. Wang, MRS Bull. **32**, 620 (2007).
[7] G. Adam and J. H. Gibbs, J. Chem. Phys. **43**, 139 (1965).
[8] L. M. Martinez and C. A. Angell, Nature **410**, 663 (2001).
[9] I. Gallino, J. Schroers, and R. Busch, J. Appl. Phys. **108**, 063501 (2010).
[10] S. Sastry, Nature **409**, 164 (2001).
[11] M. Goldstein, J. Chem. Phys. **51**, 3728 (1969).
[12] G. N. Greaves, A. L. Greer, R. S. Lakes, and T. Rouxel, Nat. Mater. **10**, 823 (2011).
[13] T. Rouxel, J. Am. Ceram. Soc. **90**, 3019 (2007).
[14] Y. Q. Cheng and E. Ma, Prog. Mater. Sci. **56**, 379 (2011).
[15] Y. Q. Cheng, E. Ma, and H. W. Sheng, Appl. Phys. Lett. **93**, 111913 (2008).
[16] N. A. Mauro, M. Blodgett, M. L. Johnson, A. J. Vogt, and K. F. Kelton, Nat. Commun. **5**, 4616 (2014).
[17] See supplementary material at http://dx.doi.org/10.1063/1.4919590 for details of the sample preparation, methods, supplementary text, and figures.
[18] I. Gallino, O. Gross, G. Dalla Fontana, Z. Evenson, and R. Busch, J. Alloys Compd. **615**, S35–S39 (2014).
[19] Z. Evenson and R. Busch, Acta Mater. **59**, 4404 (2011).
[20] Z. Evenson, T. Schmitt, M. Nicola, I. Gallino, and R. Busch, Acta Mater. **60**, 4712 (2012).
[21] Z. Evenson, *Thermodynamic and Kinetic Properties of Bulk Glass Forming Metallic Systems*, Shaker Verlag, Band 35 (Universität des Saarlandes, Saarbrücken, 2012).
[22] Z. Evenson, S. Raedersdorf, I. Gallino, and R. Busch, Scr. Mater. **63**, 573 (2010).
[23] O. Gross, "Thermodynamic and kinetic studies of the Ni-Cr-Nb-B-P and Pt-Cu/Co-Ni-P bulk metallic glass forming systems" (unpublished).
[24] W. Hembree, "Equilibrium viscosity of a $Zr_{59.3}Cu_{28.8}Al_{10.4}Nb_{1.5}$ bulk metallic glass" (unpublished).
[25] T. Egami and S. J. L. Billinge, *Unterneath the Bragg Peaks: Structural Analysis of Complex Materials*, 1st ed. (Pergamon, Oxford, 2003).
[26] J. Ding, M. Xu, P. F. Guan, S. W. Deng, Y. Q. Cheng, and E. Ma, J. Chem. Phys. **140**, 064501 (2014).
[27] H. Lou, X. Wang, Q. Cao, D. Zhang, J. Zhang, T. Hu, H. Mao, and J.-Z. Jiang, Proc. Natl. Acad. Sci. U. S. A. **110**, 10068 (2013).
[28] A. Hirata, P. Guan, T. Fujita, Y. Hirotsu, A. Inoue, A. R. Yavari, T. Sakurai, and M. Chen, Nat. Mater. **10**, 28 (2011).
[29] D. B. Miracle, Nat. Mater. **3**, 697 (2004).
[30] H. W. Sheng, W. K. Luo, F. M. Alamgir, J. M. Bai, and E. Ma, Nature **439**, 419 (2006).
[31] M. D. Ediger, Annu. Rev. Phys. Chem. **51**, 99 (2000).